Microtubule Dynamics In Vivo: A Test of Mechanisms of Turnover

Paul J. Sammak, Gary J. Gorbsky, and Gary G. Borisy

Laboratory of Molecular Biology, University of Wisconsin, Madison, Wisconsin 53706

Abstract. Clarification of the mechanism of microtubule dynamics requires an analysis of the microtubule pattern at two time points in the same cell with single fiber resolution. Single microtubule resolution was obtained by microinjection of haptenized tubulin (fluorescein-tubulin) and subsequent indirect immunofluorescence with an antifluorescein antibody. The two time points in a single cell were, first, the time of photobleaching fluorescein-tubulin, and second, the time of fixation. The pattern of fluorescence replacement in the bleached zone during this time interval revealed the relevant mechanisms.

In fibroblasts, microtubule domains in the bleached zone are replaced microtubule by microtubule and not by mechanisms that affect all microtubules simultaneously. Of the models we consider, treadmilling and subunit exchange along the length do not account for this observation, but dynamic instability can since it suggests that growing and shrinking microtubules coexist. In addition, we show that the half-time for microtubule replacement is shortest at the leading edge. Dynamic instability accounts for this observation if in general microtubules do not catastrophically disassemble from the plus end, but instead have a significant probability of undergoing a transition to the growing phase before they depolymerize completely. This type of instability we call tempered rather than catastrophic because, through limited disassembly followed by regrowth, it will preferentially replace polymer domains at the ends of microtubules, thus accounting for the observation that the half-time of microtubule domain replacement is shorter with proximity to the leading edge.

ANTITUBULIN immunofluorescence provides a snapshot of the microtubule (Mt)[1] array in interphase cells and shows long fibers extending from the centrosome and perinuclear area towards the edges of the cell (Osborn and Weber, 1982). How this pattern changes over time is important in cell motility, particle transport, and other Mt-based motions such as mitosis (Roberts and Hyams, 1979) in which an understanding of Mt dynamics will help determine what role Mt's actually play.

Polarized light microscopy of the mitotic spindle in vivo demonstrated that Mt's were in a dynamic equilibrium with subunits, and suggested that subunits could exchange along the entire length with first order kinetics (Inoué and Sato, 1967; Stephens, 1973). In contrast, experiments in vitro showed Mt's grow and shorten by addition of subunits at their ends (Johnson and Borisy, 1977). At steady state, subunit exchange with polymer is characterized by two processes. One is treadmilling (Margolis and Wilson, 1978) in which net gain of subunits at the plus end is balanced by net loss at the minus end (Bergen and Borisy, 1980). The other is dynamic instability (Mitchison and Kirschner, 1984*b*) in which subunits are gained at the plus end during a growing phase and lost at the same end during a shrinking phase.

More recently, microinjection of haptenized tubulin into cells and subsequent immunocytochemistry has allowed single fiber resolution and has confirmed the in vitro results that Mt's grow by elongation at ends distal to the centrosome (the plus ends) and by initiating new growth at the centrosome (Soltys and Borisy, 1985; Schulze and Kirschner, 1986). One possible drawback of the hapten experiments was that this growth was the result of a transient increase in tubulin concentration after microinjection (Soltys and Borisy, 1985) and so might not have represented the pattern at steady state; on the other hand, the incorporation pattern was not dependent upon the concentration of microinjected tubulin, indicating that any possible perturbation was minimal (Schulze and Kirschner, 1986).

Nevertheless, it is important that experiments investigating microtubule dynamics also be carried out at steady state. Microinjection of fluorescently tagged tubulin into interphase cells and subsequent analysis of fluorescence redistribution after photobleaching showed that the average fluorescence in a small bleached spot recovered with a half-time of a few minutes (Saxton et al., 1984). The fluorescence redistribution results indicated that Mt's were indeed dynamic at steady state in vivo, but did not address the mechanism of microtubule dynamics.

In this study we combined the techniques of microinjection of fluorescently haptenized tubulin, fluorescence re-

1. *Abbreviations used in this paper:* DTAF-T, dichlorotriazinylaminofluorescein-tubulin; Mt, microtubule.

distribution after photobleaching, and hapten-mediated immunocytochemistry to analyze Mt dynamics in human fibroblasts. Hapten-mediated immunocytochemistry provided single Mt resolution rather than averages of large numbers of microtubules, and fluorescence redistribution after photobleaching permitted analysis of the mechanism of Mt replacement at steady state rather than shortly after microinjection. Two other features of our experimental design were important. After microinjection, microtubule polymer was cycled by cooling and rewarming cells to assure that Mt's were uniformly labeled at steady state. Fluorescein was the hapten in our experiments and the fluorescein antibody we have used reacted strongly with unbleached fluorescein but not with bleached fluorescein. The reduced antigenicity of the bleached fluorescein tubulin permitted us to distinguish bleached from unbleached fibers by immunofluorescence. We use the term fiber for the linear elements detected by antitubulin staining because we have not in these experiments determined at the ultrastructural level the number of microtubules corresponding to the immunofluorescent fibers seen at the light microscopic level. However, Osborn and Weber (1982) have shown in similar type fibroblasts that most but not all such fibers are single Mt's. The results from these combined techniques showed that fluorescence redistribution after photobleaching occurred by replacement of Mt's fiber by fiber in the bleached zone and that the half-time for Mt replacement was shortest at the leading edge, near Mt plus ends.

These results directly elucidate the mechanism of Mt dynamics. First, fiber-by-fiber Mt replacement cannot be explained by models calling for exchange along the length or by simpler forms of treadmilling. This result is most easily explained by dynamic instability (Mitchison and Kirschner, 1984*a*, *b*) in which growing and shrinking Mt's coexist and interconvert infrequently. Second, the faster Mt replacement near the leading edge can be explained by a significant probability for a shrinking MT to undergo a transition back to a growing phase (Chen and Hill, 1985), thus increasing the likelihood of Mt domain replacement near the plus end. We suggest such incomplete depolymerization and dynamic instability be referred to as tempered rather than catastrophic.

Materials and Methods

Cell Culture

All tissue culture reagents were obtained from Gibco (Grand Island, NY) except as noted. Human neonate foreskin fibroblasts, line 356 (a gift from Dr. R. DeMars, Department of Genetics, University of Wisconsin) were cultured in F-10 supplemented with 20 mM Hepes, 15% FBS (HyClone Laboratories, Sterile Systems, Inc., Logan UT) and antibiotics at 37°C, 5% CO_2. In preparation for an experiment, trypsinized cells were plated onto a 22-mm square coverslip which had been carbon coated while a 400-mesh locator-grid (Ted Pella, Inc., Tustin, CA) was used as a mask to form a pattern in the carbon film. After a minimum of 24 h, coverslips with actively dividing and motile cells were transferred to a 40-mm stainless steel dish with an 18-mm hole in the bottom, and adhered with a bead of silicone vacuum grease (Dow Corning Corp., Midland, MI). Leibovitz's L-15 medium supplemented with 20 mM Hepes, pH 7.2, 15% FBS, and antibiotics was used for all manipulations at atmospheric CO_2.

Protein Preparation

Microtubule protein was obtained from porcine brain by cycles of assembly and disassembly (Borisy et al., 1975). Pure tubulin was prepared from microtubule protein by DEAE-cellulose column chromatography (Vallee and Borisy, 1978). Dichlorotriazinylaminofluorescein-tubulin (DTAF-T) was prepared as described earlier (Soltys and Borisy, 1985) with a few modifications. Reagent dye to tubulin ratio was 40:1 during a 10-min, 37°C incubation, after which the preparation was sedimented through 20% glycerol in 100 mM Pipes, pH 6.94, 1 mM EGTA, 0.1 mM $MgCl_2$, 1 mM GTP (PEMG), dialyzed against 0°C PEMG, and further purified by two cycles of polymerization at 37°C in 10% DMSO and depolymerization at 0°C without DMSO with differential centrifugation (Borisy et al., 1975). Yields were typically >50%. Upon repeated cycling DTAF-T yields were comparable to underivatized tubulin yields. Depolymerized DTAF-T at 8 mg/ml in PEMG with <1.25% DMSO was stored in liquid nitrogen. Protein concentration was determined by the method of Lowry et al. (1951). Dye concentrations were determined by absorption at 490 nm using a molar absorption coefficient of 27,000 (Leslie et al., 1984). The dye-to-protein ratio of injected protein was 1:1. Microtubule fidelity was determined by light and electron microscopic morphology and the ability to copolymerize with endogenous tubulin in microinjected cells. Additional evaluations of the probe DTAF-T can be found in references (Keith et al., 1981; Wadsworth and Sloboda, 1983; Soltys and Borisy, 1984; Leslie et al., 1984; Salmon et al., 1984*a*, *b*; Saxton et al., 1984; Soltys and Borisy, 1985).

Microinjection

Before microinjection, DTAF-T was spun for 30 min at 20,000 *g*, 0°C to clarify the solution. Pipettes (World Precision Instruments, Inc., New Haven, CT) were pulled on a vertical puller (David Kopf Instruments, Tujunga, CA), and 1/2λ DTAF-T was loaded at the pipette shank with a syringe inserted from the back. Air pressure was provided by a gas tight syringe (Hamilton Co., Reno, NV) which provided carefully regulated flow rates. A Leitz micromanipulator (E. Leitz, Inc., Rockleigh, NJ) and a Zeiss IM-35 inverted microscope (Carl Zeiss, Inc., Thornwood, NY) were used for micromanipulations. Injected volumes were estimated to be between 5 and 20% of the total cell volume.

Cooling and Rewarming

After microinjection, cells were transferred to fresh L-15 at 0°C for 20 min or longer to depolymerize Mt's (Brinkley and Cartwright, 1975; see Results) and then moved to a 37°C incubator for 30 min or longer to reassemble Mt's that were then uniformly made of copolymerized DTAF-T and endogenous tubulin. Cells were then photobleached at 25°C in a Rose chamber (Rose et al., 1958).

Photobleaching

The photobleaching apparatus was assembled according to the methods of Petersen et al. (1986). An Argon ion laser (model 2020; Spectra-Physics Inc., Mountain View, CA) and a Zeiss IM 35 microscope were anchored to a vibration isolation table (Newport Research Corp., Mountain View, CA). A 200-mm focal length cylindrical lens was positioned to produce a focused, 4 × 57 μm beam cross section in the specimen plane when a neofluar 100×, 1.3 NA objective was used. The beam was measured by photographing the fluorescence from a film of 5 μg/ml fluorescein mixed in epoxy and sandwiched between a coverslip and a microscope slide, where the concentration of fluorescein was approximately that expected in cells injected with DTAF-T and the beam power was the same as that delivered to injected cells. The $1/e^2$ width of the beam was 4 μm as determined by the method of Schneider and Webb (1981). Beam energy was determined by measurement with a photosensor in the laser head and corrected for the reflectivity of mirrors, lenses, and filters. The exposure time was controlled with an electronic shutter (Vincent Associates, Rochester, NY). All micrographs were made with Tri-X film developed in HC-110, pushed 1/2 to 1 stop.

Immunofluorescence

After photobleaching, cells were rinsed 4× in PHEM buffer (60 mM Pipes, 25 mM Hepes, 10 mM EGTA, 2 mM $MgCl_2$, pH 6.9), extracted for 90 s in 0.15% Triton X-100 in PHEM supplemented with 5 μg/ml taxol (National Cancer Institute, Bethesda, MD) (Schliwa and van Blerkom, 1981), fixed for 2 min in 2% glutaraldehyde in PHEM, and then reduced with 5 mg/ml $NaBH_4$ for 5 min. Double label immunofluorescence staining was performed as previously described (Soltys and Borisy, 1985) except that the rhodamine anti-rat secondary antibody was used at a dilution of 1:200 to reduce the tubulin stain intensity and prevent cross talk from the rhodamine-tubulin channel to the fluorescein-DTAF channel. The rabbit antifluorescein antibody is described in Gorbsky et al. (1987). The fluorescein and

rhodamine images were recorded after the sequential staining was completed.

Cells were mounted in a poly-vinyl alcohol anti-bleaching solution that provided good protection from photobleaching and excellent phase contrast. Coverslips were mounted on slides, dried overnight, and stored at −20°C. Phase and fluorescence were preserved for up to 1 yr. The medium contained 12 ml 0.2 M Tris, pH 8.5, 6 ml methanol, 6 g DMSO, 2.4 g Monsanto poly-vinyl alcohol, grade 20–30 (Monsanto Co., St. Louis, MO; but now manufactured by Air Products & Chemicals Inc., Allentown, PA; Vinol 205). The mixture was enclosed in a tube, heated in a boiling water bath for 10 min, and stored at −20°C. The day of use, para-phenylene diamine hydrochloride was added to an aliquot at 2 mg/ml.

Data Analysis

Cells were evaluated for position of the bleached zone and number of fluorescent fibers in the bleached zone by measurements on negatives at 333× with a 10× magnifier and micrometer reticule. The precision of displacement measurements was 1 μm. The width of the bleach zone, 5 ± 2 μm, was marked by the edge of a zone of reduced antifluorescein staining and varied with the portion of the bleaching beam that hit the cell; the intensity profiles of the width and length of the beam were gaussian. The bleaching beam was generally parallel to a broad flat phase dark edge of the cell and was perpendicular to a line from the nucleus to this cell edge. The displacement of the center of the bleached zone from a centrally located point on the irregular cell edge was measured on micrographs of fixed cells where possible, but in cells where no trace of the bleached zone remained, the direct fluorescence image of the bleached zone was compared to a phase-contrast micrograph taken at the time of photobleaching. For Fig. 5, the number of fluorescent fibers in the bleach zone was estimated from the negatives and each cell was judged to be in one of four classes: no fluorescent fibers, few fluorescent fibers (five or less), many fluorescent fibers (more than five but not all fibers), and complete recovery (identity between antifluorescein and antitubulin images). Because of microtubule bundling and less than ideal staining, exact counts were not possible. Pairs of prints were evaluated neighborhood by neighborhood and fluorescent material in the antifluorescein image was scored as an Mt only if it showed antitubulin staining as well. An Mt was scored as bleached if the ratio of its intensity in the antifluorescein and antitubulin micrographs was small compared to the ratio of nearby fibers outside the bleached zone. In Figs. 4 and 5, reversal prints were enlarged from a Tech-pan 2415 internegative made from the original negatives. Microtubule tracings onto clear acetate were made from these final prints. Tracings were made in 2-cm^2 regions at a time, first from the antifluorescein micrographs and then the antitubulin micrographs. Not all Mt's are represented, especially in congested areas. Curves were fitted to the data by the method of least squares, and are accompanied by standard error of estimates.

Image Analysis

One negative (Fig. 3 *a*) which printed poorly was computer enhanced to improve contrast and image density. The negative was imaged with a Dage SIT camera (Dage-MTI, Inc., Michigan City, IN) and processed with a Quantex 9200 image processor (Quantex Corp., Sunnyvale, CA). Photographs from a monitor (Sierra Scientific Corp., Mountain View, CA) were taken with a Nikon FE-2 (Nikon, Inc., Garden City, NY) on Tech pan 2415 film and developed with technidol liquid developer (Eastman Kodak Co., Rochester, NY).

Results

General Experimental Design

The aim of the experiments was to determine the mechanism of Mt turnover in living fibroblasts. To distinguish between possible models for the turnover process, we felt that the Mt pattern at two time points in the same cell had to be evaluated. The first time point was marked by laser light irradiation of a band across the cell and the second by the time of fixation. All Mt's in the irradiated zone were photobleached and thus any fibers detected later, after fixing and staining, with a bleached domain were present at the first time point. Of course, in each cell, we know the Mt pattern at two time points only within the bleached zone. Outside of the bleached zone we have no information about Mt permanence or turnover. However, by bleaching a large number of cells at different positions within the cell and with different replacement times, a composite picture of the Mt dynamics in cells can be obtained.

Temperature Cycling

It was necessary to ensure that any nonfluorescent fibers were actually bleached and not simply resistant to DTAF-T uptake. Subjecting the Mt's to a cycle of depolymerization and repolymerization by cooling and rewarming microinjected cells, as diagrammed in Fig. 1, assured that all Mt's were assembled from the same subunit pool containing a constant mole fraction of labeled tubulin. Antitubulin immunofluorescence shows that after 4 min at 0°C, no microtubules remained in 356 cells (data not shown). For photobleaching experiments, cells were routinely cooled 20 min. When rewarmed 1.3 min at 37°C, Mt's extended to the cell edge and presented a pattern similar to cells rewarmed at 37°C for 20 min and to uncooled cells (data not shown). Before photobleaching, cells were routinely warmed 30 min, to allow a return to steady state. Under these conditions the rate of polymer gain and loss was extraordinarily fast, approaching 1 μm/s and Mt regrowth was primarily centrosomal. In DTAF-T-injected cells, antifluorescein staining was uniform in intensity along Mt's indicating uniform incorporation of DTAF-T within the precision of our immunofluorescence (see Figs. 3–5).

An additional advantage of this protocol is that it ensured that all photobleached Mt's would be approximately the same age, as measured from the time of formation. This would mitigate the possibility that the age of individual Mt's might affect their stability (Gundersen, G. G., and J. C. Bulinski, manuscript submitted for publication).

A second factor that could be associated with enhanced Mt stability is the amount of detyrosinated α-tubulin incorporated into Mt's (Gundersen, G. G., and J. C. Bulinski, manuscript submitted for publication). However, immunostaining for detyrosinated tubulin generally showed low levels in 356 fibroblasts and did not reveal an Mt subset enriched in detyrosinated tubulin (data not shown).

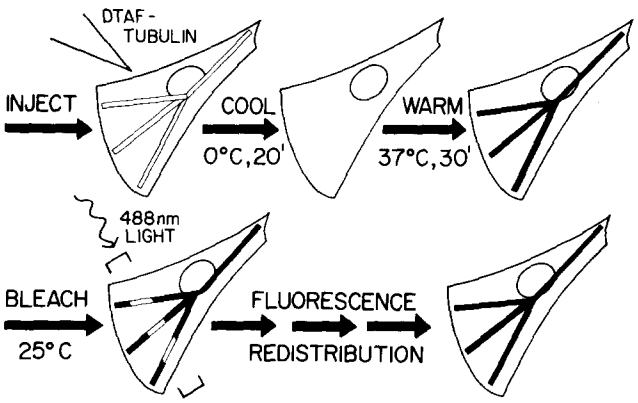

Figure 1. Experimental protocol. Cells were injected with DTAF-T, temperature cycled to produce uniform labeling, photobleached with a bar of laser light, and then incubated for various times before fixing to detect intermediate stages of fluorescence redistribution. Filled lines represent fluorescent Mt's and open lines represent photobleached Mt's. See text for details.

Factors That Might Perturb Fluorescence Replacement

Cell-to-cell variation in Mt dynamics might be expected depending on degree of motility, gross morphology, Mt bundling, and overall vitality. To minimize this variability, cells were selected that were of average size, with a broad flat lamella with a phase-dark edge that was typical of an active leading lamella. Cells with this morphology did indeed advance in 24 of 25 cells evaluated for motility after photobleaching and fixing. Cells with irregular shapes or thin processes were avoided as Mt bundling was often seen in these structures.

The bleached zone was positioned behind this leading edge, parallel to the edge and in front of the nucleus, as indicated in Fig. 1. The bleaching beam was made wide enough to extend across the cell in most instances in order to eliminate the chance that fluorescence recovery could occur by unbleached fibers moving laterally into the bleached zone. The pulse duration, 500 ms, was selected as the minimum time needed to register the direct fluorescence by eye and film. The beam energy selected, 13 mW, was high enough to just adequately bleach the fluorescence without additionally causing Mt damage and was adequate to distinguish bleached from unbleached Mt's by immunofluorescence.

At 13 mW, the potential for cell damage was evaluated by several criteria. Thermal damage can be caused by nonradiative de-excitation of the dye. Assuming an absorption coefficient of 2.7×10^3 $M^{-1}cm^{-1}$ for DTAF at pH 6.9 (Leslie et al., 1984), a quantum efficiency of 0 (all absorbed light produces heat), an intracellular DTAF concentration of 4 μM, and a cell height of 2 μm, we calculate, according to the method of Bloom and Webb (1984), that the temperature rise under our experimental conditions would be negligible—0.14°C. Heat conduction effectively limits the temperature increase.

In addition to heating, photochemical reactions, most likely via oxygen and not directly due to the excited fluorophore (Bloom and Webb, 1984; Foote, 1976), could still damage irradiated cytoplasm. Cells not containing DTAF-T were irradiated for 30 s at 26 mW, 116 times more energy than that used for photobleaching, and showed no morphological changes. Vesicles and particularly mitochondria showed no sign of paling or shape changes as has been produced by 532-nm irradiation (Berns et al., 1981). No Mt breakage was detected by immunofluorescence. In cells both injected with DTAF-T and photobleached at 13 mW for 500 ms, no morphological changes or mitochondrial paling was observed. Mt breakage was not seen in any of the 71 cells presented in this study that were fixed between 2.5 and 65 min after bleaching. However, Mt damage was produced in experiments not presented here where higher beam energies were used or when immotile cells were bleached. Broken Mt's, restricted to the bleached zone, were observed in a few cells fixed as long as 30 min after bleaching. This photodamage was not observed in the experiments presented here.

Particles occasionally were observed to move through the bleached zone shortly after bleaching, and injected and irradiated cells continued to locomote, moving 9.6 ± 2.7 μm/h at 25°C. It is possible that cell motility and shape changes could distort the bleached zone and affect our measurements. In the 29 cells that showed partial Mt replacement, the overall shape of the bleaching beam was still evident in the distribution of bleached Mt domains in fixed cells (see Figs. 4 and 5). Cell displacement during the interval between bleaching and fixing was <10% of the distance between the bleached zone and the leading edge. Thus, distortion of the bleached zone due to motility at 25°C was minimal.

Reduced Binding of Antifluorescein to Bleached DTAF Mt's

The difference between bleached and unbleached Mt's in living cells can be detected by direct micrography (data not shown), but currently the best detection of the fibrous Mt pattern is by antifluorescein and antitubulin immunofluorescence. However, for the success of these experiments it was essential that the fluorescein antibody not react with the bleached fluorescein so that bleached Mt's could be recognized by the absence of antifluorescein staining. This was first evaluated by bleaching cells previously fixed and stained with antitubulin and a secondary antibody conjugated with fluorescein. Fluorescein bleaching was permanent, showing no recovery of fluorescence over minutes or days as previously reported (Peters et al., 1974). When subsequently stained with antifluorescein and a secondary antibody conjugated with rhodamine, Mt's in the bleached zone were much dimmer than unbleached Mt's outside the zone, in both the fluorescein and rhodamine channels.

Antifluorescein staining was next evaluated in DTAF-T–injected cells as shown in Fig. 2. Fig. 2, *a* and *b*, was taken at the time of photobleaching. The wedge seen in Fig. 2 *b* is the direct fluorescence from the DTAF-T in the cell whose outline is seen in Fig. 2 *a*. The irradiated area was <3% of the total cell area. The pattern of light recorded is a function of the shape of the illuminating beam and the distribution of DTAF-T in the beam path. The narrowing edge of the bleach beam produces the wedge shape. This cell was lysed after 2 min, and fixed 3.5 min after bleaching. The antifluorescein (Fig. 2 *c*) and antitubulin (Fig. 2 *d*) staining showed that the Mt's were still present in the bleached zone, but the bleached fibers were only dimly labeled with antifluorescein.

Fluorescence Redistribution Over Time Occurs Fiber by Fiber

Cells were fixed shortly after bleaching and were evaluated for details of the fluorescence replacement process (Fig. 3). The cell in Fig. 3, *a–f*, was lysed 3 min and fixed 4.5 min after photobleaching. Fig. 3 *a*, taken at the time of photobleaching was made by overlaying negatives of the phase-contrast and direct fluorescence images. The original fluorescence negative of this one cell was too thin to overlay and was darkened and contrast enhanced as explained in Materials and Methods. Note that the direct fluorescence was contained in a vertical bar but had structure complementary to the Mt pattern seen in Fig. 3, *b* and *c*, taken after the cells were fixed. At low magnification a general impression of the bleached zone is gained that is influenced mostly by the average brightness. Compare the pairs of low magnification prints for the three cells in Fig. 3 (*b* and *c*; *h* and *i*; *n* and *o*). These immunofluorescent cell images, recorded at progressively later times after photobleaching, show that fluorescence became redistributed into the bleached zone as previously reported (Saxton et al., 1984).

At higher magnification, the outline of the bleached zone is less distinct, but the fibrous nature of the fluorescence is

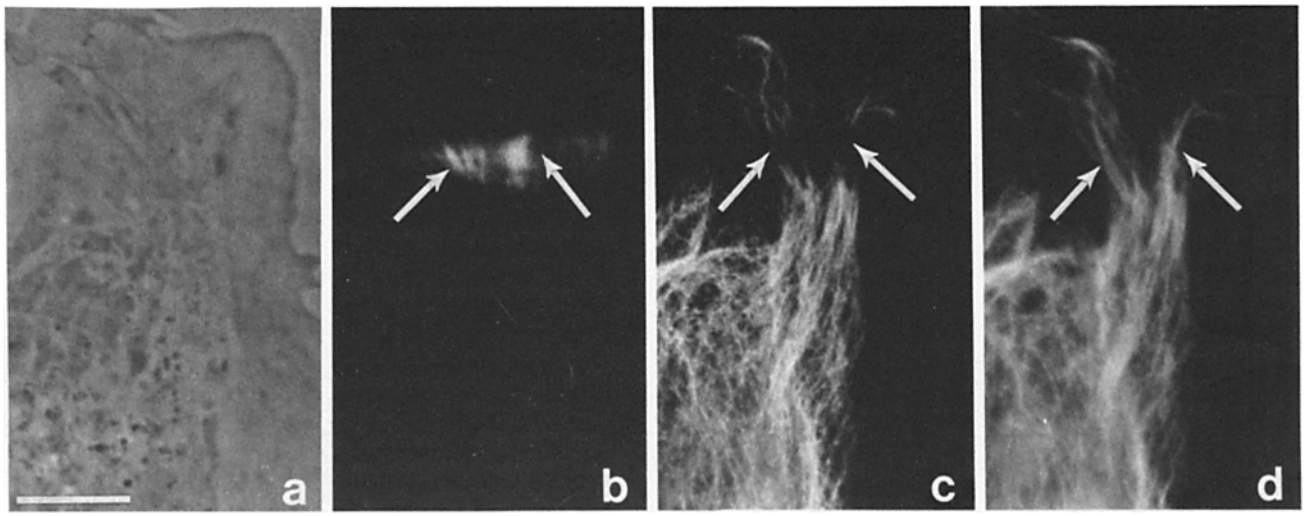

Figure 2. Photobleached Mt's fail to bind antifluorescein antibody. (*a* and *b*) Phase-contrast and fluorescence micrographs taken at the time of photobleaching show the cell edge and position of the direct fluorescence during irradiation. (*c* and *d*) Indirect immunofluorescence of the same cell fixed after 3.5 min; antifluorescein antibody fails to bind in the bleached zone (*c*) even though Mt's are still present by antitubulin staining (*d*). The arrows show two Mt bundles (*d*) whose primary fluorescence when irradiated (*b*) complements the staining of unbleached fibers (*c*). Bar, 10 μm.

clearer, and the pattern of redistribution can be evaluated. With reversal prints, dark Mt's are shown on a light background, and although this is different from the microscope image, dark lines are much easier to perceive and compare.

The antifluorescein staining in the bleached zone of the first cell (Fig. 3 *d*) was not completely absent, but was greatly reduced. Because the brightness of the staining depends on Mt density in a fiber as well as bleaching, the difference between antifluorescein and antitubulin staining of a given fiber is important as well as differences between different fibers in the antifluorescein image. A fiber was scored as bleached if the ratio of its intensity in the antifluorescein and antitubulin images was small compared to the ratio of nearby fibers outside the bleached zone. By this criterion, all fibers in the bleached zone of Fig. 3 *d* were scored as bleached at 4.5 min after photobleaching as illustrated in the interpretive diagram shown in Fig. 3 *f*. Arrowheads (Fig. 3, *d–f*) indicate one example of a bleached fiber.

The second cell of Fig. 3 (*g–l*) was fixed 16.5 min after photobleaching and shows a mixed population of bright (*arrow*) and dim (*arrowhead*) fibers in the bleached zone. Since all fibers were bleached, fluorescent Mt domains in the bleached zone were assembled during the 16.5-min interval between bleaching and fixing. The pattern observed at this time point revealed fluorescent fibers side by side with nonfluorescent fibers, indicating that redistribution of fluorescence occurred predominantly fiber by fiber; fibers did not appear to recover their fluorescence gradually and uniformly. In all cells showing intermediate stages of recovery, bleached fibers can clearly be seen next to unbleached fibers (see especially Figs. 3, *j* and *k*, and 4, *p* and *q*, for additional examples). This suggests that the major mechanism of fluorescence replacement in the bleached zone is the progressive replacement of nonfluorescent fibers by fluorescent fibers. The bleached fibers might also slowly increase their fluorescence over time. A direct comparison of the brightness of bleached fibers in different cells is not possible because of the unevenness of staining. However, coexistence of adjacent bleached and fluorescent Mt's excludes a mechanism of uniform, gradual replacement of fluorescence as a major mechanism of Mt dynamics in fibroblasts.

Many, but not all fibers detected by immunofluorescence are single Mt's (Osborn and Weber, 1982). The bleached fibers analyzed here would in some instances be single Mt's but some fibers were certainly Mt bundles. The arrowhead in Fig. 3 *j* points to such a bundle. Note also that highly bundled Mt's here, and in Fig. 4, were not replaced earlier or later than the thinner fibers in the same bleached zone. In spite of the limits of detection of light microscopy, the pattern of Mt replacement over time was certainly fiber by fiber and most likely, Mt by Mt.

The third cell of Fig. 3 (*m–r*) was fixed 55.5 min after the entire width of the cell was bleached (Fig. 3 *m*). All fibers were fluorescent as shown by the identity between the antifluorescein (Fig. 3 *p*) and antitubulin (Fig. 3 *q*) micrographs, suggesting complete Mt replacement in 1 h. No markers remained for the position of the bleach bar and it was no longer possible to identify the original bleached fibers.

To examine the possibility that fluorescence recovery in the bleached zone occurred by movement of fibers, cells were examined for longitudinal displacement of bleached domains on fluorescent fibers. Inspection of negatives for 71 cells showed no noticeable longitudinal movement of some bleached Mt domains with respect to others. Similarly, reversal prints of the six cells shown in Figs. 3 and 4 were carefully evaluated at 3,000× for 20 μm on either side of the bleach zone and no clear examples of bleached Mt domains were seen away from the general region of the bleach zone. These observations, though limited by nonuniform staining and high Mt density, provide evidence against treadmilling as a significant explanation for the redistribution of fluorescence.

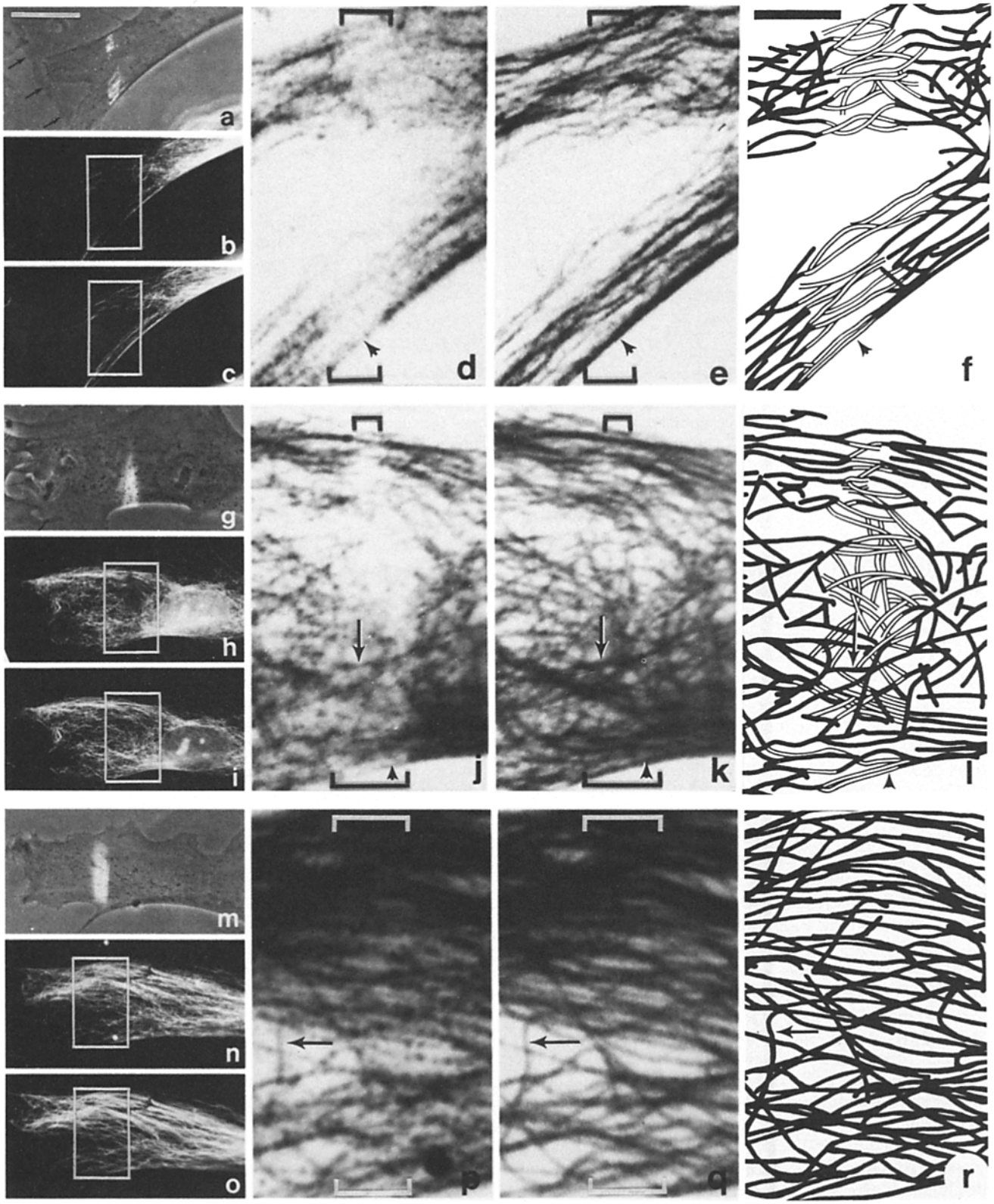

Figure 3. Fluorescence redistribution over time. Cells fixed 4.5 (*a–f*), 16.5 (*g–l*), and 55.5 (*m–r*) min after photobleaching, each at 27 ± 3 μm from the leading edge. First, *a*, *g* and *m* are superimposed micrographs of phase-contrast and direct fluorescence images taken at the time of bleaching. Next are antifluorescein (*b*, *h*, and *n*) and antitubulin (*c*, *i*, and *o*) micrographs taken after fixing and staining. The boxed regions are enlarged, antifluorescein (*d*, *j*, and *p*) followed by antitubulin (*e*, *k*, and *q*) micrographs. Brackets show the bleached zone. An interpretive diagram follows (*f*, *l*, and *r*) where unbleached fibers are represented as filled lines and bleached fibers as open lines. Arrowheads point to bleached fibers and arrows show new, fluorescent fibers. A dark square of carbon film from the 400-mesh locator pattern (see Materials and Methods) is indicated by the small arrows in the phase-contrast image (*a*). Bars: (*a*) 20 μm; (*f*) 5 μm.

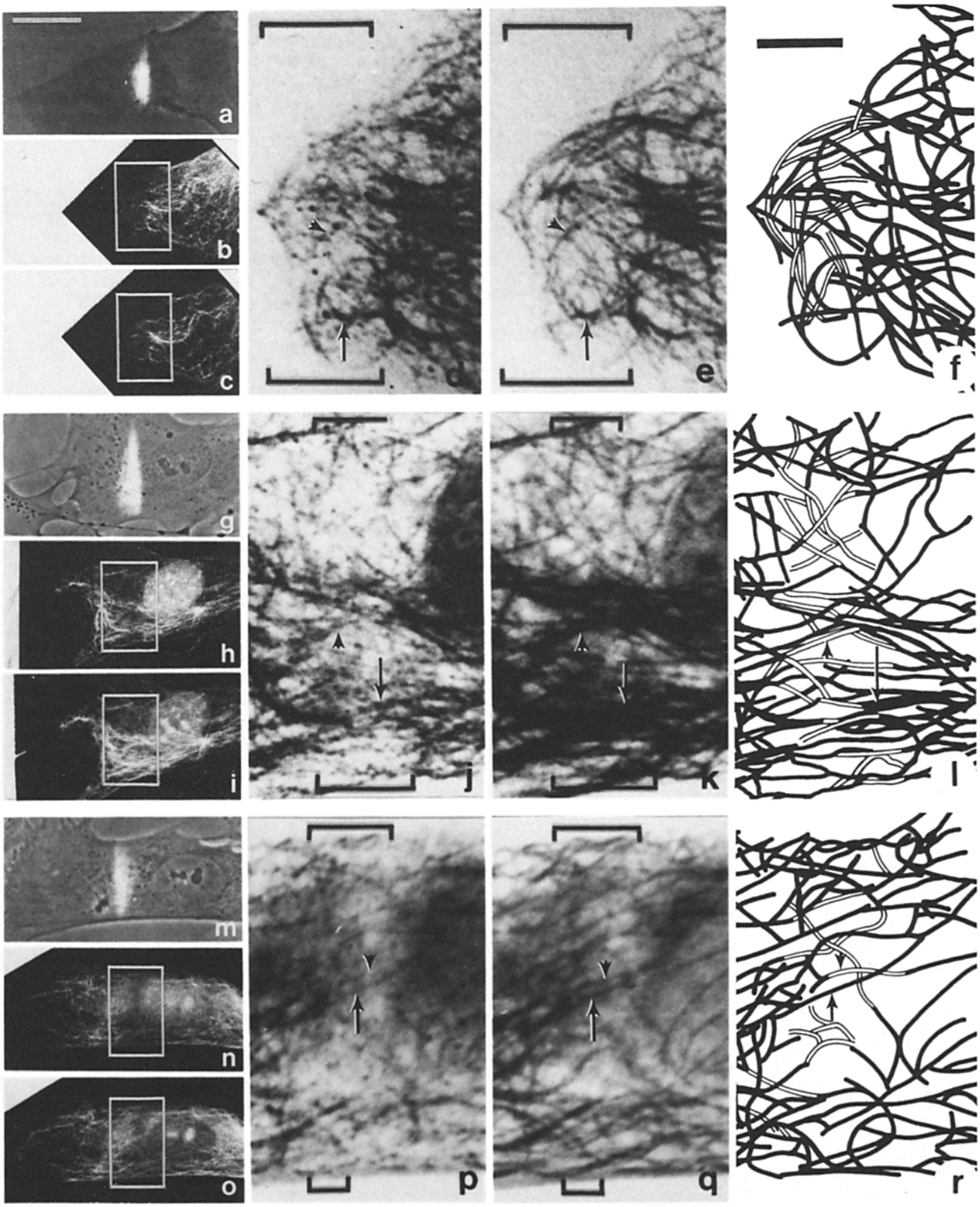

Figure 4. Partial fluorescence replacement at different locations in the cell. Cells fixed 7 (*a–f*), 22 (*g–l*), and 35 (*m–r*) min after photobleaching. Bleached zones are 4, 23, and 42 μm from the leading edge, respectively. First, *a*, *g*, and *m* are superimposed phase-contrast and direct fluorescence micrographs taken at the time of bleaching; next are antifluorescein (*b*, *h*, and *n*) and antitubulin (*c*, *i*, and *o*) micrographs taken after fixing and staining. The boxed regions are enlarged, antifluorescein (*d*, *j*, and *p*), followed by antitubulin (*e*, *k*, and *q*) micrographs. Brackets show the bleached zone. An interpretive diagram follows (*f*, *l*, and *r*) where unbleached fibers are represented as filled lines and bleached fibers as open lines. Arrowheads point to bleached fibers, and arrows show new, fluorescent fibers. Bars: (*a*) 20 μm; (*f*) 5 μm.

Microtubule Replacement Times Depend on Distance from the Leading Edge

Although at any given distance from the leading edge, Mt replacement was progressive, the time course of replacement was not monotonic. Examples of cells exhibiting partial fluorescence replacement at increasing distance from the leading edge are shown in Fig. 4. Bright direct fluorescence (*a*, *g* and *m*) confirmed that Mt's in the bleached zone were irradiated and, therefore, bleached. However, many of the fibers in the bleached zone 7 min (Fig. 4 *d*), 22 min (Fig. 4 *j*), and 35 min (Fig. 4 *p*) after bleaching were stained with the antifluorescein antibody indicating Mt replacement. These fluorescent Mts must have been assembled during the time interval between bleaching and fixation. As seen in Fig. 3, the pattern of replacement was fiber by fiber. However, in contrast to the results shown in Fig. 3, roughly the same number of bleached fibers remained in each of these three cells fixed at progressively longer times after bleaching. Lack of a tight correlation between Mt replacement and time suggested a second variable affected the redistribution. Since Mt growth normally appears first at the centrosome and at Mt ends distal to the centrosome (Soltys and Borisy, 1985; Schulze and Kirschner, 1986), proximity of the bleached zone to the centrosome or the leading edge might influence replacement times. The distances of the center of the bleach bar from the leading edge, 4 μm (Fig. 4 *a*), 23 μm (Fig. 4 *g*), and 42 μm (Fig. 4 *m*), and the time intervals, 7, 22, and 35 min, respectively, roughly correlated with each other for these cells with approximately the same degree of Mt replacement. This suggested that time and distance could be compensating factors for microtubule replacement. Since replacement increased progressively with time, we inferred that replacement might be slower the further a microtubule domain was from the leading edge.

To examine the effect of time and position on microtubule replacement more systematically, cells were bleached at various positions from the leading edge and fixed at various times and then examined for microtubule replacement. Cells were categorized as displaying little, partial, or complete replacement (Fig. 5), and the results show both variables determine Mt replacement. Cells of increasing degree of recovery (Fig. 5, *A–C*, respectively) were plotted comparing the time between bleaching and fixing to the distance of the bleached zone from the leading edge. Straight lines, determined by linear regression from each data set, were drawn for simplicity to illustrate the dependence of Mt replacement times on position. A linear dependence cannot be established from this data set. A square root dependence, for example, could also be supported. This dependence is supported not only by the correlation of data on any one graph, but also by the lack of overlap of data points among the three graphs. In Fig. 5 *A*, the time for little or no Mt replacement is weakly dependent on distance from the leading edge with an increase in Mt turnover time of 0.25 min for each μm from the edge. The turnover time at any position had a standard error of estimate of ±5.2 min. In Fig. 5 *B*, the time for partial Mt replacement (that is, more than five but not all fibers fluorescent) is more strongly dependent on position with an increase in recovery time of 0.55 min/μm with a standard error of estimate of ±6.1 min. This line represents an upper bound for the half-time for Mt replacement; most cells in Fig. 5 *B* have a large proportion of fluorescent Mt's in the bleached zone. As an example, this estimate of the half-time 10 μm behind the leading would be 13 ± 6.1 min. The solid line in Fig. 5 *C* shows that the average time for complete Mt turnover increases 1.2 min/μm. However, the position of this line is somewhat artificial. There is some minimum time for complete Mt replacement and cells incubated longer than

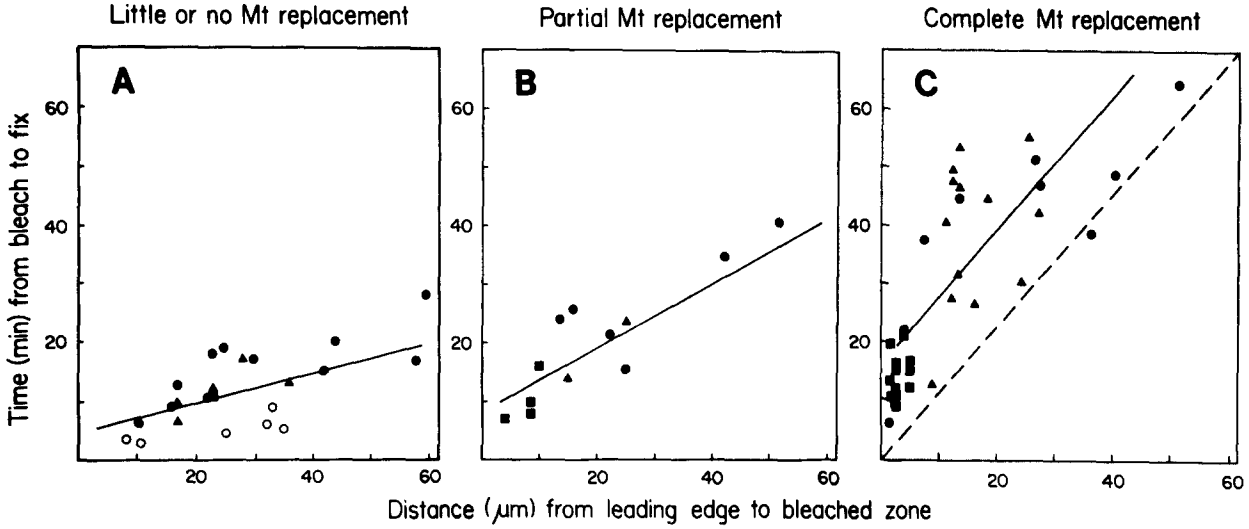

Figure 5. Mt replacement time depends on distance from the leading edge. Cells from three experiments (*circles*, *squares*, *triangles*) are plotted here with respect to three variables: distance between bleach zone and leading edge is plotted on the abscissa; time interval between bleaching and fixing is plotted on the ordinate; and cells of different degrees of recovery are plotted in different graphs. *A* shows cells with 1–5 fluorescent fibers (*closed symbols*) or no fluorescent fibers in the bleach zone (*open symbols*). *B* shows cells with more than five but not all fibers fluorescent. *C* shows cells with all fibers fluorescent. The lines were determined by linear regression and estimate the replacement time for little, partial, and complete recovery, respectively, as a function of distance from the leading edge. The line for partial recovery represents an upper bound for the half time for Mt replacement. The dotted line in *C* is parallel to the linear regression average but passes through the origin, and shows the position dependence of the minimum time for complete Mt replacement.

this time will all show complete Mt replacement. The dotted line in Fig. 5 *C* has the same slope as the line determined by linear regression but falls through the origin and represents an estimate of the increase in the minimum time for complete Mt turnover as a function of distance from the leading edge. Fig. 5 *C* also shows that the half-time for the loss of old Mt's as well as the gain of new Mt's is shortest near the leading edge since no bleached Mt domain remained in these cells.

Since Mt replacement times increased away from the leading edge, one might expect decreasing replacement times away from the centrosome. However, the correlation of recovery time with distance of the bleached zone from the centrosome was poor (data not shown). This could reflect that the time to replace bleached Mt domains is determined by the distance from Mt plus ends (at the leading edge) and not by the distance to Mt minus ends (at the centrosome). However, since not all Mt's are attached to the centrosome, this conclusion is not firm.

In addition, when the times between bleaching and fixing for cells with complete Mt replacement were plotted versus cell size (distance between the centrosome and leading edge), no correlation of Mt replacement time and total length was found (not shown). In terms of replacement time, large cells and long Mt's were not different from small cells and short fibers for a given distance between bleached zone and leading edge.

Discussion

We have analyzed Mt dynamics in human fibroblasts in order to distinguish among three principal mechanisms of Mt replacement, namely subunit exchange along the length, treadmilling, and dynamic instability. To test these models, the Mt pattern at two time points had to be evaluated in the same cell with single fiber resolution. We have combined microinjection of haptenized tubulin and subsequent indirect immunofluorescence using fluorescein as the hapten to provide single fiber resolution, and fluorescence replacement after photobleaching and subsequent fixation to demarcate a time interval in single cells. The pattern of fluorescence replacement in the bleached zone during this time interval addresses the relevant mechanisms (Fig. 6). Gradual and uniform reappearance of tagged tubulin in all Mt's would support subunit exchange along the length of the Mt. Longitudinal translocation of labeled domains into the bleached zone from the plus edge, or movement of the bleached zone en bloc towards the centrosome would support Mt treadmilling. The appearance of fully labeled fibers alongside unlabeled ones would support dynamic instability. The pattern of Mt replacement in the bleached zone can be summarized by three key observations: Mt's in the bleached zone were replaced asynchronously (that is, fiber by fiber); the half-time for the appearance of new Mt domains in the bleached zone was shortest near Mt plus ends; the half-time for the disappearance of older, bleached Mt domains was shortest near Mt plus ends.

The first model, subunit exchange along the length (Inoué and Sato, 1967) suggests DTAF-T would intercalate into the Mt lattice and produce a gradual and uniform increase in antifluorescein labeling of bleached Mt domains. However, Mt domains in the bleached zone did not uniformly recover their fluorescence. There were two classes of fibers in each cell: bleached and fluorescent. Although brightness varied among the fibers bleached by the less intense wings of the gaussian bleaching beam, newly fluorescent fibers in each cell were measurably brighter than bleached ones. This observation also excludes aberrant wall binding of DTAF-T as a mechanism of fluorescence replacement. Although uniform tubulin intercalation into all Mt's is excluded, we cannot formally exclude heterogeneous incorporation into selected Mt's. However, heterogeneous intercalation seems unlikely, since microinjected tubulin labeled Mt ends and not the entire length of selected Mt's (Soltys and Borisy, 1985; Schulze and Kirschner, 1986). Mt breaking and annealing (Rothwell et al., 1986) also is not the major mechanism of fluorescence replacement in these experiments, since, by and large, bleached Mt domains were continuous across the bleached zone.

The second model, Mt treadmilling (Margolis et al., 1978), in its simplest form would suggest that synchronous growth at Mt plus ends near the leading edge and shortening at Mt minus ends at the centrosome moves the bleach zone en bloc towards the centrosome. However, synchronous Mt treadmilling cannot explain the pattern of fluorescence replacement in the bleached zone since the replacement is asynchronous and occurs fiber by fiber. Asynchronous treadmilling could be produced if some minus ends were prevented from disassembling, say by attachment to the centrosome, and if the attachment itself were also regulated. Asynchronous treadmilling would then move the bleached domains of some Mt's out of the bleached zone towards the nucleus. We did not observe movement of bleached Mt domains towards the nucleus, although Mt congestion prevented us from tracing Mt's >20 μm away from the bleached zone. In addition, asynchronous treadmilling would move the entire length of an Mt and so the replacement of bleached

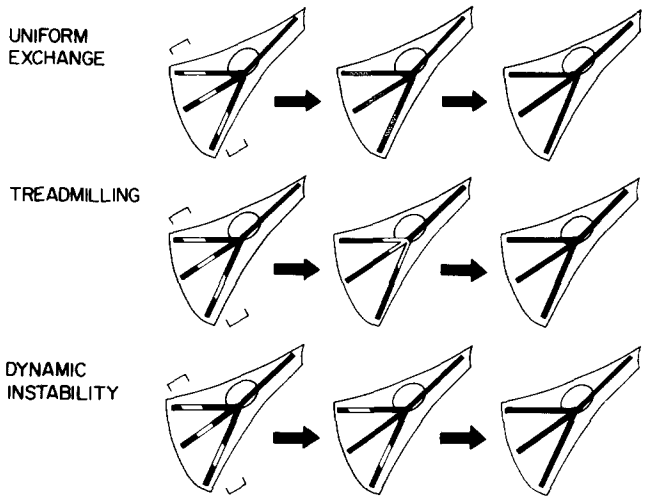

Figure 6. Three models. Replacement of bleached Mt domains (*open lines*) illustrates the predictions of three models. Uniform exchange predicts a gradual increase in fluorescence as DTAF-T intercalates into bleached domains. Treadmilling predicts that bleached domains translocate longitudinally and are disassembled at the minus end. Dynamic instability predicts growing and shrinking microtubules coexist and that bleached and fluorescent fibers should appear side by side.

domains would be independent of position of the bleached zone. Since this prediction clearly runs counter to our observations, asynchronous treadmilling is not likely to be a major mechanism of Mt turnover.

The third model, dynamic instability, suggests that fluorescent fibers and bleached fibers should appear side by side. As seen in Figs. 3 and 4, the pattern of fluorescence replacement in the bleached zone supports dynamic instability as the major mechanism of Mt replacement. Dynamic instability stipulates that growing and shrinking Mt's coexist and that interconversion between these two phases occurs infrequently. In the steady state in vitro, Mt plus ends in the growing phase elongate slowly at 1.9 μm/min, while in the shrinking phase they shorten rapidly at 12 μm/min (Mitchison and Kirschner, 1984 *b*). At steady state, Mt's spend more time in the growing than shrinking phase in order to balance polymer gain and loss. Kristofferson et al. (1986) suggested that an Mt that initiates disassembly almost always disassembles catastrophically. They showed that biotin-labeled domains within predominantly unlabeled Mt's maintained a constant average length while Mt's increased in length and decreased in number. Partial disassembly and subsequent regrowth with unlabeled tubulin should have produced a decline in the average length of biotin–tubulin domains. Since the average length remained unchanged, it would seem that the Mt length lost during an excursion of disassembly was substantially longer than the 21-μm biotin domains. In contrast to this result, Horio and Hotani (1986) showed by direct darkfield observation of dynamic instability in vitro that the average excursion length was small with Mt's losing 2–4 μm during the shortening phase. These observations also showed that both Mt ends underwent phase changes, but that the plus end was dominant, changing phase more frequently and undergoing greater length fluctuations.

Can catastrophic disassembly of Mt's explain that the half-time for both Mt gain and loss in cells is shortest near the leading edge? This is not likely. Mt loss would be independent of position since catastrophic instability would disassemble the entire Mt length (see Fig. 7).

Could variations in half-times for Mt replacement in different parts of the cell be the result of Mt populations of differing turnover times? If a subpopulation of longer-lived Mt's tended to exist in the cell center while shorter-lived Mt's extended to the edge, the average Mt turnover time would increase towards the cell center. Enhanced Mt stability has been associated with increased Mt age or increased levels of detyrosinated tubulin, but in the experiments presented here, Mt age was approximately the same and the level of anti-detyrosinated tubulin staining was uniformly low and did not reveal an Mt subset (see Results). However, we have no direct evidence against the existence of a subpopulation of long-lived Mts and it is possible that they could contribute to the increase in turnover time towards the cell center. Additional experiments are needed to measure the lifetimes of individual Mt's and to confirm tempered instability.

Because catastrophic instability does not seem able to account for the shorter replacement times near the leading edge, we examined how replacement time might depend on the probability of interconversion between the growing and shrinking phases. Catastrophic instability presumes the probability of conversion is low or essentially zero so that a shrinking Mt would disassemble completely. We suggest that

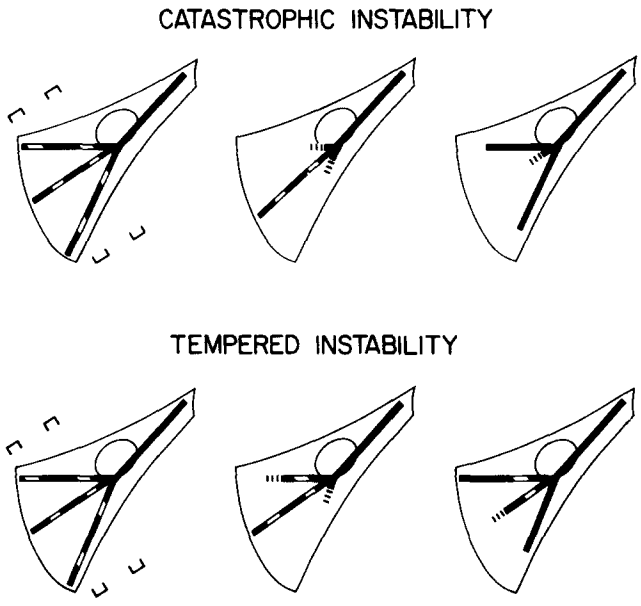

Figure 7. Catastrophic vs. tempered Mt instability. Replacement of Mt domains in bleached zones at two distances from the leading edge illustrates the predictions of catastrophic and tempered instability. Catastrophic instability predicts the half-time for Mt loss is independent of the distance from the leading edge since complete Mt disassembly removes bleached domains in both positions. Tempered instability predicts that the half-time for Mt loss is shorter near the leading edge since partial shortening preferentially removes bleached domains near the leading edge.

in vivo the probability for an Mt undergoing a phase transition is non-zero for each subunit disassembled. Then, the chance of a shrinking Mt undergoing a phase transition would stochastically increase with the length of polymer disassembled. Mt's in fibroblasts are commonly 20–50 μm long. For Mt's of this length, we assume the probability of conversion from the shrinking phase to the growing phase to be significantly different from zero. We term this kind of dynamic instability tempered rather than catastrophic because an episode of disassembly on any individual Mt would frequently be incomplete, and growth could resume (Fig. 7).

Tempered instability assumes Mt's rapidly shorten from the plus end until they stop and then grow. Estimates of this transition probability in vitro range from a 50% chance for a phase change for 20 μm of diassembly (Mitchison and Kirshner, 1984 *b*) to a 50% chance for regrowth after 6 μm of disassembly (Chen and Hill, 1985). Tempered instability predicts Mt's would be replaced asynchronously as observed. It also predicts that bleached Mt domains near the leading edge would disappear more rapidly since the chance of stopping a shrinking Mt would increase away from the original plus end and in effect, protect bleached Mt domains far from Mt ends. New fluorescent Mt's would appear more frequently near the leading edge as many fibers would partially disassemble and then regrow. The half-time for Mt replacement would be shortest at the leading edge and increase towards the cell center. Thus, the predictions of tempered instability agree with our experiments.

Mt turnover might be a regulated process. Different mechanisms, such as breaking and annealing, treadmilling, and dynamic instability may all exist under particular conditions

and serve different purposes: dynamic instability for fast rescaffolding, treadmilling possibly in association some form of movement, breaking and reannealing for fiber rearrangement or reorientation. However, tempered dynamic instability seems sufficient to account for Mt replacement in these experiments which also show that the other models are insufficient explanations. Nevertheless, these experiments cannot exclude contributions from other mechanisms of Mt dynamics especially far from the leading edge.

The transition probability for converting a shrinking Mt into a growing one should depend on concentration of tubulin and GTP, the activity of microtubule-associated proteins and possibly ion concentrations, and could itself be regulated to control the rate of Mt dynamics. A high probability for a shrinking Mt being converted into a growing Mt would mean Mt's at the leading edge would turn over very rapidly compared to Mt's closer to the nucleus. This would favor rapid change in the Mt pattern at the active leading edge. Lower transition probabilities would mean longer Mt domains would disassemble in the same span of time. This could be used for example when a fibroblast changes direction and needs to remove Mt's that extend to the old leading edge and assemble new Mt's towards a new leading edge.

The turnover of MT's during mitosis is much faster than in interphase (Saxton et al., 1984). The mechanism of Mt dynamics could still be fundamentally the same throughout the cell cycle since tempered instability predicts that short interphase Mt domains near the plus end could have turnover times comparable to the turnover times of short mitotic Mt's. Further, changes in the turnover times could be accounted for in terms of transition probabilities. Reducing the probability for converting a shrinking Mt into a growing Mt would mean Mts would completely disassemble more often, thus reducing the turnover time.

The dramatic reduction of the average Mt length at the interphase–prophase transition could be produced by a change in the growing-to-shrinking phase transition probability. Increasing the probability for converting a growing Mt into a shrinking Mt would reduce the average Mt length. These examples illustrate how the regulation of the two transition probabilities might be an important point of control of Mt dynamics and Mt patterns.

We would like to thank Eliot Elson for guidance in setting up the optics on the laser bench; Bohdan Soltys for his advice on the preparation of DTAF-T and carbon-coated coverslips; Jim Pawley for guidance in video electronics; Steven Limbach, Lori Vaskalis, and Leslie Rabas for expert illustration and photography; and Patricia Hanson for preparation of this manuscript.

This work was supported by National Institutes of Health grant GM25062 (G. G. Borisy) and the Integrated Microscopy Facility for Biomedical Research (NIH RR00570).

Received for publication 5 June 1986, and in revised form 28 October 1986.

References

Bergen, L. G., and G. G. Borisy. 1980. Head to tail polymerization of microtubules in vitro. *J. Cell Biol.* 84:141–150.

Berns, M. W., J. Aist, J. Edwards, K. Straks, J. Girton, P. McNeill, J. B. Rattner, M. Kitzes, M. Hammer-Wilson, L.-H. Liaw, A. Siemens, M. Koonce, S. Peterson, S. Brenner, J. Burt, R. Walter, P. J. Bryant, D. van Dyk, J. Coulombe, T. Cahill, and G. S. Berns. 1981. Laser microsurgery in cell and developmental biology. *Science (Wash. DC).* 213:505–513.

Bloom, J. A., and W. W. Webb. 1984. Photodamage to intact erythrocyte membranes at high laser intensities. *J. Histochem. Cytochem.* 32:608–616.

Borisy, G. G., J. M. Marcum, J. B. Olmstead, D. B. Murphy, and K. A. Johnson. 1975. Purification of tubulin and associated high molecular weight proteins from porcine brain and characterization of microtubule assembly *in vitro*. *Ann. NY Acad. Sci.* 253:107–132.

Brinkley, B. R., and J. Cartwright. 1975. Cold-labile and cold stable microtubules in the mitotic spindle of mammalian cells. *Ann. NY Acad. Sci.* 253:428–439.

Chen, Y., and T. L. Hill. 1985. Theoretical treatment of microtubules disappearing in solution. *Proc. Natl. Acad. Sci. USA.* 82:4127–4131.

Foote, C. S. 1976. Photosensitized oxidation and singlet oxygen: consequences in biological systems. *Free Radicals in Biology.* 2:85–133.

Gorbsky, G. J., P. J. Sammak, and G. G. Borisy. 1987. Chromosomes move poleward in anaphase along stationary microtubules that coordinately disassemble from their kinetochore ends. *J. Cell Biol.* In press.

Horio, T., and H. Hotani. 1986. Visualization of the dynamic instability of individual microtubules by dark-field microscopy. *Nature (Lond.).* 321:605–607.

Inoué, S., and H. Sato. 1967. Cell motility by labile association of molecules. *J. Gen. Physiol.* 50:259–292.

Johnson, K., and G. G. Borisy. 1977. Kinetic analysis of microtubule assembly *in vitro*. *J. Mol. Biol.* 117:1–31.

Keith, C. H., J. R. Feramisco, and M. Shelanski. 1981. Direct visualization of fluorescein-labeled microtubules *in vitro* and in microinjected fibroblasts. *J. Cell Biol.* 88:234–240.

Kristofferson, D., T. Mitchison, and M. Kirschner. 1986. Direct observation of steady-state microtubule dynamics. *J. Cell Biol.* 102:1007–1009.

Leslie, R. J., W. M. Saxton, T. J. Mitchison, B. Neighbors, E. D. Salmon, and J. R. McIntosh. 1984. Assembly properties of fluorescein-labeled tubulin *in vitro* before and after fluorescence bleaching. *J. Cell Biol.* 99:2146–2156.

Lowry, O. H., N. J. Rosebrough, A. L. Farr, and R. J. Randall. 1951. Protein measurement with the Folin-phenol reagent. *J. Biol. Chem.* 193:265–275.

Margolis, R. L., and L. Wilson. 1978. Opposite end assembly and disassembly of microtubules at steady-state *in vitro*. *Cell.* 13:1–8.

Margolis, R. L., L. Wilson, and B. I. Kiefer. 1978. Mitotic mechanism based on intrinsic microtubule behaviour. *Nature (Lond.).* 272:450–452.

Mitchison, T., and M. Kirschner. 1984*a*. Microtubule assembly nucleated by isolated centrosomes. *Nature (Lond.).* 312:232–237.

Mitchison, T., and M. Kirschner. 1984*b*. Dynamic instability of microtubule growth. *Nature (Lond.).* 312:237–242.

Osborn, M., and K. Weber. 1982. Immunofluorescence and immunocytochemical procedures with affinity purified antibodies: tubulin-containing structures. *Methods Cell Biol.* 24:97–131.

Peters, R., J. Peters, K. H. Tews, and W. Bähr. 1974. A microfluorimetric study of translational diffusion in erythrocyte membranes. *Biochim. Biophys. Acta.* 367:282–294.

Petersen, N. O., S. Felde, and E. L. Elson. 1986. Measurement of lateral diffusion by fluorescence photobleaching recovery. *Handbook of Experimental Immunology.* 4th ed. D. M. Weir, editor. Blackwell, Oxford. 1:24.1–24.22.

Roberts, K., and J. S. Hyams, editors. 1979. *Microtubules.* Academic Press, Inc., New York.

Rose, G. G., C. M. Pomerat, T. O. Shindler, and J. B. Trunnell. 1958. A cellophane-strip technique for culturing tissue in multipurpose culture chambers. *J. Biophys. Biochem. Cytol.* 4:761–764.

Rothwell, S. W., W. A. Grasser, and D. B. Murphy. 1986. End to end annealing of microtubules in vitro. *J. Cell Biol.* 102:619–627.

Salmon, E. D., R. J. Leslie, W. M. Saxton, M. L. Karow, and J. R. McIntosh. 1984*a*. Spindle microtubule dynamics in sea urchin embryos: analysis using a fluorescein-labeled tubulin and measurements of fluorescence redistribution after laser photobleaching. *J. Cell Biol.* 99:2165–2174.

Salmon, E. D., W. M. Saxton, R. J. Leslie, M. L. Karow, and J. R. McIntosh. 1984*b*. Diffusion coefficient of fluorescein-labeled tubulin in the cytoplasm of embryonic cells of a sea urchin: video image analysis of fluorescence redistribution after photobleaching. *J. Cell Biol.* 99:2157–2164.

Saxton, W. M., D. L. Stemple, R. J. Leslie, E. D. Salmon, M. Zavortink, and J. R. McIntosh. 1984. Tubulin dynamics in cultured mammalian cells. *J. Cell Biol.* 99:2175–2186.

Schliwa, M., and J. van Blerkom. 1981. Structural interaction of cytoskeletal components. *J. Cell Biol.* 90:222–235.

Schneider, M. B., and W. W. Webb. 1981. Measurement of submicron laser beam radii. *Applied Optics.* 20:1382–1388.

Schulze, E., and M. Kirschner. 1986. Microtubule dynamics in interphase cells. *J. Cell Biol.* 102:1020–1031.

Soltys, B. J., and G. G. Borisy. 1984. Correlative light and electron microscopy of microinjected fluorescent tubulin or actin. *J. Cell Biol.* 99(4, Pt. 2):196*a*. (Abstr.).

Soltys, B. J., and G. G. Borisy. 1985. Polymerization of tubulin in vivo: direct evidence for assembly onto microtubule ends and from centrosomes. *J. Cell Biol.* 100:1682–1689.

Stephens, R. E. 1973. Thermodynamic analysis of mitotic spindle equilibrium at active metaphase. *J. Cell Biol.* 57:133–147.

Vallee, R. B., and G. G. Borisy. 1978. The non-tubulin component of microtubule protein oligomers. *J. Biol. Chem.* 253:2834–2845.

Wadsworth, P., and R. D. Sloboda. 1983. Microinjection of fluorescent tubulin into dividing sea urchin cells. *J. Cell Biol.* 97:1249–1254.